Industrial Crops & Products 251 (2026) 124135

Contents lists available at ScienceDirect

Industrial Crops & Products

journal homepage: www.elsevier.com/locate/indcrop

Bio compatibilizers from brewer's spent grain for biocomposite production

Gioele Foltran [a,b,*], Silvia Conca [c], Valentina Beghetto [b,c,d]

[a] Department of Architecture and Industrial Design, University of Campania "Luigi Vanvitelli", Aversa, Italy
[b] Department of Molecular Sciences and Nanosystems, University Ca' Foscari of Venice, Via Torino 155, Mestre 30172, Italy
[c] Crossing S.r.l., Viale della Repubblica 193/b, Treviso 31100, Italy
[d] Consorzio Interuniversitario per le Reattività Chimiche e La Catalisi (CIRCC), Via C. Ulpiani 27, Bari 70126, Italy

ARTICLE INFO

Keywords:
Waste valorisation
Bio compatibilizers
Brewer's spent grain
Bio-composite
PBS

ABSTRACT

This study demonstrates that the lipid fraction of brewer's spent grain (BSG), traditionally overlooked in polymer composite applications, can be chemically converted into bio-based compatibilizers while the lignocellulosic fraction simultaneously serves as reinforcement. Two model bio-additives, 6-*O*-linoleyl-α-*D*-glucopyranosyl-β-*D*-fructofuranoside (SE) and 9,10:12,13-diepoxyoctadecanoic acid (EA), were synthesized starting from linoleic acid, main component of BSG lipid fraction, and their performance as additives was evaluated. Poly(butylene succinate) (PBS) was selected as the biopolymer matrix, and PBS/BSG blends (70/30 wt/wt) containing SE or EA at concentrations between 2 and 8 wt% were prepared. Thermal, mechanical, chemical, and morphological analyses (DSC, TGA, ATR-FTIR, and SEM) showed that PBS/BSG biocomposites containing 6 wt% SE exhibited the best overall performance, highlighting an effective compatibilizing effect. Conversely, the addition of 6 wt% EA mainly increased surface hydrophobicity, raising the contact angle to approximately 80°, compared to PBS and PBS/BSG blends (<70 °). The lipid fraction of BSG was extracted using ethyl acetate or supercritical CO_2, achieving yields up to 97%, and subsequently chemically modified to obtain the corresponding sucrose ester (SES) and epoxide (SEO). PBS/BSG blends containing 6 wt% of SES or SEO were then prepared. SES-based biocomposites showed improved thermal stability, mechanical properties, and interfacial adhesion compared to PBS/BSG blends, confirming a strong compatibilizing action. In contrast, SEO imparted pronounced hydrophobicity, with contact angles exceeding 100°, while only modest variations in mechanical properties were observed. Bio-fragmentation tests confirmed enhanced biodegradability for all modified composites. Overall, this work demonstrates that brewer's spent grain can simultaneously serve as a reinforcing filler and as a renewable source of functional compatibilizers, providing an integrated strategy for the production of high-performance fully bio-based composites.

1. Introduction

Fossil-based plastics have been widely used since the mid-twentieth century and are now essential materials in many sectors due to their low cost, durability, and versatile properties (Chandran et al., 2020; Environment, U.N, 2021). Over the past decades, their global production has increased sharply, reaching approximately 400 Mt in 2024, with growth rates exceeding those of the global gross domestic product (European Bioplastics, 2024; Nayanathara Thathsarani Pilapitiya and Ratnayake, 2024; Plastics Europe, 2024). This extensive production has resulted in significant environmental concerns, including high greenhouse gas emissions, estimated at more than 252 Mt of CO_2 in 2022, as well as the widespread accumulation of micro- and nanoplastics in ecosystems (Beghetto et al., 2023; Jambeck et al., 2015; Qin et al., 2022; Walker and Fequet, 2023). These phenomena are increasingly associated with adverse ecological effects and potential risks to human health (Allouzi et al., 2021; Singh and Tiwari, 2025; Winiarska et al., 2024).

In this context, biodegradable polymers such as polylactic acid (PLA), poly(butylene succinate) (PBS), and poly(butylene adipate-co-terephthalate) (PBAT) have emerged as promising alternatives to conventional plastics and have driven the expansion of the bioplastics market, which was valued at approximately 15.57 billion USD in 2024 (Grand View Research, 2024). Despite this growth, biopolymers still represent only about 0.5% of total global plastic production. Their broader implementation is currently limited by factors such as feedstock availability, production costs, and processing constraints (Coppola et al.,

* Corresponding author at: Department of Architecture and Industrial Design, University of Campania "Luigi Vanvitelli", Aversa, Italy.
E-mail address: gioele.foltran@unicampania.it (G. Foltran).

https://doi.org/10.1016/j.indcrop.2026.124135
Received 5 February 2026; Received in revised form 14 July 2026; Accepted 9 August 2026
Available online 18 August 2026

2021; European Bioplastics, 2024).

One effective strategy to overcome these limitations involves the development of biocomposites, in which biodegradable polymers are combined with agro-industrial byproducts. This approach not only reduces material costs but also improves sustainability by valorising waste streams and decreasing the consumption of virgin biopolymers (Beghetto et al., 2026; Canzian et al., 2026; Latos-Brozio et al., 2025; Manu et al., 2022; Saffian et al., 2021; Santhosh et al., 2024; Silva et al., 2014).

Large quantities of agricultural residues are still disposed of through landfilling or low-value applications, generating environmental and economic burdens (Lackner and Besharati, 2025; Rao et al., 2024; Visco et al., 2022). Their use as fillers in biocomposites contributes to waste valorisation while simultaneously reducing land use associated with biopolymer feedstock cultivation (Faheem and Khan, 2025; Pęśko and Masek, 2025). However, a key challenge in the production of biocomposites is the poor interfacial compatibility between hydrophobic polymer matrices and hydrophilic lignocellulosic fillers. This mismatch often leads to weak interfacial adhesion, resulting in reduced mechanical performance and morphological heterogeneity (Fredi and Dorigato, 2024; Hejna et al., 2026; Imre and Pukánszky, 2013). To address this issue, several compatibilization strategies have been proposed. Reactive extrusion using compounds such as acrylic acid, methylene diphenyl diisocyanate, poly(hydroxyester ether), poly(vinyl alcohol), or maleic anhydride has been shown to improve matrix–filler interactions (Fang et al., 2024; Olonisakin et al., 2025; Surendren et al., 2022). Nevertheless, these approaches often involve toxic or hazardous reagents, limiting their environmental compatibility and industrial appeal. As a result, non-reactive blending in the presence of suitable additives, acting as compatibilizers, is increasingly considered a safer and more cost-effective alternative (Santandrea and Beghetto, 2025; Sin et al., 2013).

Compatibilizers typically consist of block copolymers or low-molecular-weight amphiphilic compounds containing functional segments with affinity for both the polymer matrix and the filler surface. In some cases, partially miscible polymers may also serve this function (Chinn et al., 2024; Jeepery et al., 2023; Self et al., 2022; Shakoor Shar et al., 2023). A wide range of bio-based substances, including epoxidized plant oils, cardanol derivatives, citrate or isosorbide esters, starch, cellulose, citric acid, and glycerol, have been successfully employed as compatibilizers in polymer blends and biocomposites (Beghetto, 2025a; Choo et al., 2023; Dominguez-Candela et al., 2022; Dutta et al., 2021; Intranuwong et al., 2025; Ma et al., 2024; Saabome Samuel Muobom and Sangmyung University, Seoul, South Korea, 2020; Song et al., 2023). Considering that the market for bio-based polymer additives is expected to reach 2.2 billion USD by 2029 (MarketsandMarkets, 2025), the development of novel bio-based compatibilizers represents a significant opportunity to replace fossil-derived additives and enable fully sustainable biocomposite systems (Bardella et al., 2024; Beghetto, 2025a).

Within this framework, brewer's spent grain (BSG) is a particularly attractive resource. BSG is the main byproduct of the brewing industry and is generated in large quantities, estimated at approximately 39 Mt per year worldwide (Souza et al., 2025). Although it is traditionally used as animal feed, increasingly restrictive regulations are expected to limit this application, leading to higher disposal rates and associated environmental impacts (Baiano and Fiore, 2025; Kavalopoulos et al., 2021).

Previous studies have demonstrated the feasibility of using BSG as a lignocellulosic bio filler in combination with various biodegradable polymers (Belardi et al., 2025; Hejna et al., 2025; Visco et al., 2025). However, the performance of these bio composites remains strongly dependent on effective compatibilization, as the poor interfacial adhesion between the hydrophilic filler and the hydrophobic polymer matrix often limits their mechanical and thermal properties (Visco et al., 2026).

While considerable research has focused on the lignocellulosic fraction of BSG, as well as its protein, fiber and carbohydrate content, its lipid fraction has received comparatively little attention, despite representing approximately 10 wt% of the dry biomass. In parallel, increasing interest has been devoted to the valorisation of lipid-rich agro-industrial residues as renewable feedstocks for the production of plasticizers, compatibilizers and other functional polymer additives (Beghetto, 2025b). However, to the best of our knowledge, the conversion of BSG lipids into compatibilizers for polymer composites has not yet been reported. Exploiting this underutilized fraction therefore provides an opportunity to extend the valorisation of BSG beyond its conventional use as a filler, while simultaneously increasing the bio-based content and sustainability of composite materials.

Based on these considerations, we hypothesized that the lipid fraction of BSG, which is generally neglected in polymer composite production, could be chemically transformed into amphiphilic molecules capable of improving matrix-filler interactions in PBS/BSG composites.

To the best of our knowledge, this is the first study demonstrating the extraction and chemical modification of BSG lipids for this purpose. To test this hypothesis, model additives, namely a sucrose ester (SE) and an epoxidized fatty acid (EA), were first synthesized from commercial linoleic acid and subsequently reproduced using lipids extracted directly from BSG (Henkin et al., 2025). The use of commercial linoleic acid provided well-defined model compounds, allowing the proposed molecular design to be evaluated under controlled conditions before applying the same synthetic strategy to the more complex lipid fraction extracted from BSG. After validating the compatibilizing performance of the model additives, the corresponding BSG-derived products (SES and SEO) were prepared and evaluated in PBS/BSG biocomposites. This strategy enabled a systematic comparison between model additives and their BSG-derived counterparts.

The central concept of this work is therefore not merely the development of a new bio-based compatibilizer, but the integrated valorisation of two chemically distinct fractions of the same agricultural residue. In the proposed approach, the lignocellulosic fraction is directly employed as reinforcing filler, whereas the lipid fraction is chemically upgraded into functional amphiphilic additives that improve matrix-filler interactions. By assigning complementary functions to different fractions of the same biomass, this strategy maximizes resource utilization while reducing the need for externally sourced additives.

Subsequently, lipids were extracted from BSG using ethyl acetate or supercritical CO_2, hydrolysed, and chemically modified to obtain the corresponding sucrose ester (SES) and epoxidized oil (SEO), as reported in Scheme 1. All products were characterised by FT-IR NMR and elemental analysis. Additionally, iodine value of the lipid extracts was measured according to the procedure reported in the literature (Guillén and Ruiz, 2003).

Poly(butylene succinate) (PBS) was selected as the polymer matrix based on previous studies (Visco et al., 2025), and PBS/BSG biocomposites (70/30 wt/wt) containing different concentrations of the prepared additives were produced. The effect of these bio-based compatibilizers on the thermal, mechanical, morphological, surface, and biodegradation properties of the resulting biocomposites was systematically investigated.

2. Materials and methods

Brewer's spent grain (BSG) was supplied pre-dried form (residual moisture content approximately 2 wt%) by Birrificio Messina (Italy) originated from lager beer production using barley malt. Poly(butylene succinate) (PBS) was provided by Xinjiang Blue Ridge Tunhe Sci.&Tech. Co. and had a density of 1.26 g/cm^3, melting temperature of 115 °C and melt flow rate (MFR) of 22 g/10 min (190 °C/2.16 kg). All reagents and solvents were bought from Merk (Milano, Italy) and used without further purification. Chemical characterization of the synthesized additives and BSG-derived products was performed by ATR-FTIR on a PerkinElmer Spectrum Two Spectrometer with a $LiTaO_3$ detector (Waltham, Massachusetts, USA). Nuclear magnetic resonance (^{1}H, ^{13}C,

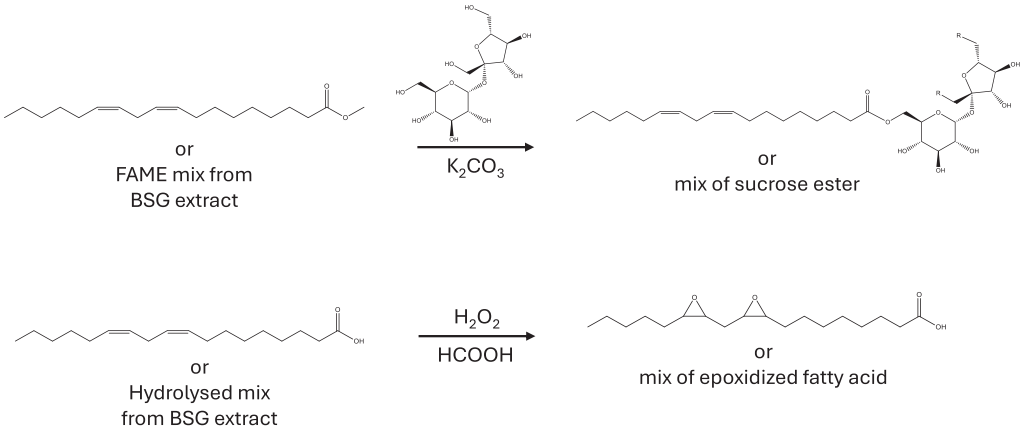

Scheme 1. Overall synthetic strategy for the production of biobased additives SE, EA, SES and SEO.

COSY, HSQC, and HMBC) spectra were recorded on a Bruker AVANCE 400 spectrometer (Bruker, Milan, Italy) operating at 400.21 MHz for ^{1}H and 101.0 MHz for ^{13}C. Elemental analysis were carried out using a Unicube analyzer (Beersel, Belgium), while LC-MS/MS analyses were performed using a Bruker qTOF instrument. (Milano, Italy).

2.1. Bio additive synthesis

2.1.1. Synthesis of 6-O-linoleyl-α-D-glucopyranosyl-β-D-fructofuranoside (Sucrose ester, SE)

Sucrose esters were prepared via transesterification reactions starting from fatty acid methyl esters, following established literature procedures (Zheng et al., 2015). Linoleic acid was first converted into its methyl ester under basic conditions, as previously reported, and subsequently used for sucrose ester synthesis. Briefly, sucrose (17.93 g, 0.05 mol) was dissolved in dimethylformamide (DMF, 0.36 L) in an Erlenmeyer flask, and potassium carbonate (6.91 g, 0.05 mol) was added. The mixture was heated to 85 °C until a clear solution was obtained. Linoleic acid methyl ester (14.69 g, 0.05 mol) was then added dropwise, and the reaction was maintained at 85 °C under stirring for 48 h. After completion, the mixture was filtered, and the resulting yellowish solid was extracted using a water/dichloromethane biphasic system. The aqueous phase was evaporated under reduced pressure to obtain the sucrose ester (10.0 g, 33% yield). Structural characterization was carried out by NMR spectroscopy, ATR-FTIR, LC–MS, and elemental analysis (Figures S9–S15, Table S1).

2.1.2. Synthesis of 9,10:12,13-diepoxyoctadecanoic acid (Epoxidized acid, EA)

The epoxidation of linoleic acid was performed following the procedure reported by Fong and Salimon (Fong and Salimon, 2012) with minor modifications. Hydrogen peroxide solution (30 wt% in water, 8.0 mL) was slowly added to a stirred solution of linoleic acid (15.0 g, 0.05 mol) in formic acid (14.0 mL) at 4 °C using an ice bath. The reaction mixture was stirred overnight. After completion, the oily phase was neutralized with 1 M NaOH and extracted with dichloromethane. The organic layer was dried under reduced pressure, yielding epoxidized linoleic acid (24.0 g, 85% yield). The product was characterized by NMR spectroscopy, ATR-FTIR, and elemental analysis (Figures S16–S21, Table S1).

2.2. Extraction and hydrolysis of BSG lipidic fraction

The lipid fraction of dry BSG was extracted using either solvent-based or supercritical fluid techniques. The recovered oil was subsequently hydrolysed and chemically modified to produce BSG-derived sucrose esters (SES) and epoxidized oils (SEO), following the same synthetic protocols described for SE and EA. All BSG-derived products were characterized by NMR spectroscopy, ATR-FTIR, and elemental analysis (Figures S28–S44, Table S1)

2.2.1. Extraction with EtOAc

The lipid fraction of BSG (particle size < 250 μm) was extracted by refluxing 5.0 g of dry BSG in ethyl acetate (EtOAc) for 24 h. After extraction, the solvent was removed under reduced pressure. The extract was analysed by ^{1}H and ^{1} ^{3}C NMR spectroscopy, two-dimensional NMR, and ATR-FTIR (Figures S22–S27). Extraction yields were calculated assuming that lipids account for approximately 10 wt% of dry BSG. Triplicate extractions of 5.0 g of BSG yielded an average of 0.38 ± 0.02 g of oil, corresponding to an extraction efficiency of approximately 75%.

2.2.2. Extraction with supercritical CO_2 ($SCCO_2$)

Supercritical CO_2 extractions were carried out using an EXTRATEX supercritical fluid extractor (Pont-Saint-Vincent, France). Samples of dry BSG (5.0 g) were extracted for 30 min at a CO_2 flow rate of 30 $g{\cdot}min^{-1}$. Extraction conditions were varied by adjusting pressure (200–300 bar) and temperature (40–70 °C), according to literature data (Lisci et al., 2024; Lisci Silvia et al., 2022). All extracts were dried overnight under ambient conditions and analysed by NMR spectroscopy (Figure S33). Reported data represent the average of at least three independent experiments for each set of conditions.

2.2.3. Hydrolysis of BSG lipid fraction

Extracted BSG oil was hydrolysed using an aqueous NaOH solution (4.5 M) under stirring at 60 °C overnight. The reaction mixture was then acidified to pH 2–3 using 5 M HCl, and the liberated fatty acids were extracted with diethyl ether. The organic phase was dried over $MgSO_4$, filtered, and concentrated under reduced pressure to obtain BSG free fatty acids (BSG-FFA), with a yield of 69%.

The degree of unsaturation was evaluated by determining the iodine value (IV), while the relative content of saturated, oleic, linoleic, and linolenic acids was calculated by ^{1}H NMR spectroscopy following the method proposed by Guillén & Ruiz (eq S1 −5) (Guillén and Ruiz, 2003).

2.3. Preparation of PBS/BSG biocomposites (PB)

Prior to processing, PBS and BSG were dried in an oven at 70 °C overnight. Dried BSG was ground using a RETSCH SM300 cutting mill and sieved with an Endecotts Minor 200 apparatus to obtain particles smaller than 250 μm (Figure S 1). PBS/BSG biocomposites (70/30 wt/wt, PB) containing different amounts of bio compatibilizer were prepared using a Brabender Plastograph EC internal mixer. All three heating zones were set at 140 °C, and the materials were mixed for 10 min at

100 rpm. The formulations are reported in Table 1. Dumbbell-shaped test specimens were fabricated via compression moulding using a Collin P200 E hydraulic press. The prepared blends were packed into perforated stainless-steel moulds with the specimen geometry and processed isothermally at 140 °C. The pressure cycle consisted of three consecutive steps: 7 min at contact pressure (0 bar), 5 min at 50 bar, and 3 min at 100 bar. Finally, the specimens underwent a 5-min cooling stage under pressure until reaching approximately 50 °C prior to demoulding. Dumbbell-shaped specimens were obtained with a useful section length of 28 mm and a cross-sectional area of 8.16 mm^2.

2.4. Bio-composites Characterization

Colour measurements were carried out using a Konica Minolta CM−2600d spectrocolorimeter with D65 illuminant and specular component excluded. Results were expressed in the CIELAB colour space (L*, a*, b*) using a white reference standard ($L^* = 91.76$, $a^* = 4.12$, $b^* = -10.9$). Measurements were performed in triplicate at three different positions for each sample. Total colour difference (ΔE) and browning index (BI) were calculated using standard equations (Eqs. 1–2). The conversion of the parameters from CIELAB to RGB space was obtained using an online converter (nixcolorsensor).

$$\Delta E = \sqrt{(L_s^* - L^*)^2 + (a_s^* - a^*)^2 + (b_s^* - b^*)^2} \quad (1)$$

$$BI = [(100 \bullet (x - 0.31))/0.17] \quad (2)$$

Where x is obtained from Eq. 3:

$$x = [(a^* + 1.75 \bullet l^*)/(5.645 \bullet l^* + a^* - 0.3012 \bullet b^*)] \quad (3)$$

The conversion of the parameters from CIELAB to RGB space was obtained using an online converter (nixcolorsensor).

Water contact angle measurements were conducted using a Celeston digital microscope. A 10 μL droplet of deionized water was deposited onto the press-moulded specimen surface, and the contact angle was measured after 10 s. Image analysis was performed using ImageJ software.

ATR-FTIR analysis was performed directly on the press-moulded specimen with a PerkinElmer Spectrum Two Spectrometer with a $LiTaO_3$ detector (Waltham, Massachusetts, USA). Spectra were normalized (Min-Max) using PerkinElmer Spectrum software; data represent the representative profile of three replicates ($n = 3$).

Thermogravimetric analyses (TGA) were performed using a STAR PT−1000 analyser (Linseis, Messgeräte, Germany) by heating samples from 30 °C to 600 °C at 10 °C·min^{-1} under nitrogen flow (20 mL·min^{-1}).

Differential Scanning Calorimetry (DSC) measurements were carried out on a Mettler Toledo DSC 3 instrument (Mettler Toledo, Milan, Italy) under nitrogen atmosphere (flow rate of 20 mL/min). Samples were heated, cooled, and reheated to evaluate melting and crystallization behaviour (temperature range from 25 °C to 160 °C, 10 °C/min). Degree of crystallinity was obtained using Eq. (4) (Phua et al., 2012):

$$\chi_c(\%) = \left(\frac{\Delta H_m}{\Delta H_0 * (1 - w)}\right) * 100 \quad (4)$$

χ_c is the degree of crystallinity (%), ΔH_m is the melting enthalpy of the sample (J/g) and ΔH_0 is the melting enthalpy of PBS having 100% crystallinity (110.3 J/g), w is the weight fraction of BSG in the composites.

Mechanical tensile tests were conducted using a Instron 34TM5 testing machine equipped with a 500 N load cell, at a crosshead speed of 10 mm·min^{-1} and controlled temperature and humidity conditions. Young's modulus (E, MPa), tensile strength (σ_b, MPa), and elongation at break (ε_b, %) were calculated from stress–strain curves.

Fracture surfaces of dumbbell-shaped specimens were analysed by scanning electron microscopy (SEM) using a Hitachi TM3000 microscope (Tokyo, Japan), operating at 5.0 kV. Samples were gold-coated prior to analysis with a K450X sputter coater (Emitech, England).

Biofragmentation tests were carried out in soil under controlled temperature and humidity conditions, following literature procedures with minor modifications (Piñeros-Hernandez et al., 2017). Degradation was assessed visually at predetermined time intervals.

Table 1
Identification code and composition of the different bio-composites tested in this work.

Sample code	PBS [wt%]	BSG [wt%]	BC [wt%]
PBS	100	0	
PB	70	30	
PB-SE2	70	30	2
PB-SE4	70	30	4
PB-SE6	70	30	6
PB-SE8	70	30	8
PB-EA2	70	30	2
PB-EA4	70	30	4
PB-EA6	70	30	6
PB-EA8	70	30	8
PB-SES	70	30	6
PB-SEO	70	30	6

PB: PBS/BSG 70/30 wt/wt; BC: Biocompatibilizer = SE: sucrose ester of linoleic acid; EA: epoxidized linoleic acid; SES: sucrose ester from solvent extracted BSG oil; SEO: epoxidized solvent extracted BSG oil.

3. Results and discussion

3.1. Design strategy of the bio-based compatibilizers

To verify the proposed compatibilization strategy, two model amphiphilic additives were first synthesized from commercial linoleic acid (LA) before extending the same protocol to lipids extracted from BSG (Scheme 1). In fact, LA according to Del Rio et al., is the most abundant acid present in the lipidic fraction of BSG and was therefore selected as model substrate for the preliminary synthesis of SE and EA (Del Río et al., 2013). Aiming to synthesize amphiphilic low molecular weight molecules to be used in non-reactive compatibilization (Imre et al., 2019), SE and EA were specifically selected as they both bear polar functional groups, which should be compatible with the BSG fraction, and apolar alkyl chains, which are similar to the polymeric matrix (Scheme 1). SE was synthesized by transesterification of linoleic methyl ester in the presence of sucrose, while EA was obtained by epoxidation of LA according to the literature (Scheme 1) (Fong and Salimon, 2012; Zheng et al., 2015). Having established the molecular design of the model compatibilizers, the same synthetic approach was subsequently applied to the lipid fraction extracted from BSG.

3.2. Extraction and synthesis of BSG-derived additives

Starting from BSG, traditional solvent extraction with ethyl acetate (EtOAc) or with environmentally sustainable supercritical CO_2 ($SCCO_2$) were carried out and efficiency in the extraction of the BSG oily fraction

Table 2
Extraction of BSG with ethyl acetate or supercritical CO_2.

Solvent	Time (h)	T (°C)	Pressure (bar)	Yield (%)[a]
EtOAc	24	77	1	75
$SCCO_2$	0.5	40	200	60
$SCCO_2$	0.5	40	300	61
$SCCO_2$	0.5	70	300	97

a) Yield in lipids was calculated considering that the lipid fraction in BGS is ~10 wt% of the weight of BSG dry sample treated (see supporting information section).

compared (see Table 2) (Ferrentino et al., 2019; Lisci et al., 2024; Lisci Silvia et al., 2022; Spinelli et al., 2016). Yield in lipid extraction were calculated based on the fact that, according to the literature, average composition of BSG is of about 17–25 wt% cellulose and hemicellulose, 25–35 wt% non-cellulosic carbohydrates, 8–28 wt% lignin, 15–24 wt% protein, and 10 wt% lipids (Del Río et al., 2013). The samples obtained with the two different extraction methods were characterized by ^{1}H NMR spectroscopy displaying for each sample characteristic signals corresponding to triglycerides (Wang et al., 2015) (see Figure S 33). Results show that when higher $SCCO_2$ pressures were used at 70 °C, extraction efficiency was almost quantitative, allowing to extract over 97% of the lipids present in BSG, in agreement with the literature (Lisci Silvia et al., 2022).

Although $SCCO_2$ extraction afforded the highest lipid recovery (97%), ethyl acetate extraction was selected for the subsequent preparation of the bio-based additives because it combines high extraction efficiency with simpler equipment requirements and easier scalability. In addition, the NMR spectra indicated comparable extract purity for both extraction methods (Figure S33). Therefore, EtOAc was considered the most suitable extraction strategy for the synthesis of the BSG-derived compatibilizers. The lipid fraction extracted from BSG was then characterized by ^{1}H NMR spectroscopy and based on the integrals of the diagnostic proton signals (Figure S22), the iodine value (IV) was determined, yielding 140.4 g I_2/100 g (Guillén and Ruiz, 2003). Moreover, the method enabled the determination of the relative proportions of saturated, oleic, linoleic and linolenic acyl groups (Fig. 1).

The recovered oil fraction was chemically modified using the same synthetic strategy adopted for the model compounds. This enabled the preparation of the BSG-derived additives SES and SEO and allowed a direct comparison between additives synthesized from commercial linoleic acid and those obtained directly from BSG. All products were characterized by NMR, FT-IR and elemental analysis (Figures S34-S44 and Table S1, Supporting Information).

Unlike the model additives prepared from pure linoleic acid, the BSG-derived products originate from a naturally heterogeneous lipid fraction containing saturated and unsaturated fatty acids together with minor lipidic components. Consequently, the resulting compatibilizers are expected to consist of a distribution of structurally related amphiphilic molecules rather than a single defined compound, which is expected to influence their behaviour at the polymer-filler interface.

3.3. Compatibilization of PBS/BSG composites

3.3.1. Mechanical properties

Dumbbell specimens of PB and all biocomposites containing the additives were used to measure tensile strength (σ_b, MPa), elongation at break (ε_b, %) and Young's modulus (E, MPa, see Fig. 2). As for other biocomposites reported in the literature (Salmah et al., 2013), the addition of BSG leads to a significant drop of σ_b (15.71 ± 0.87 MPa), ε_b (4.0 ± 0.9%) and an increase in the stiffness of PB (951 ± 37 MPa), compared to PBS (34.2 ± 1.1 MPa, 454.0 ± 27.3% and 265.8 ± 12.1 MPa respectively).

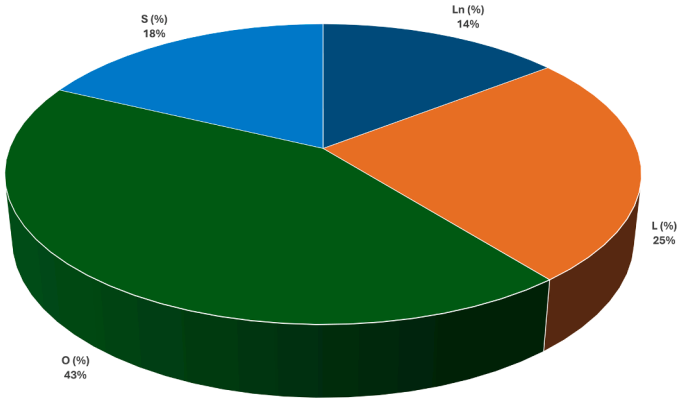

Fig. 1. Relative percentages of saturated (S), oleic (O), linoleic (L), and linolenic (Ln) acyl groups in BSG oil extracts.

The mechanical performance of the PBS/BSG composites was significantly modulated by both the additive concentration and the specific chemical structure of the additives, highlighting distinct behaviours between the sucrose ester family (SE, SES) and the epoxidized fatty acid series (EA, SEO). The addition of SE induced a typical plasticizing effect, characterized by a significant drop in stiffness (down to 463.47 MPa for PB-SE4) and a transient increase in ductility at low loadings (PB-SE2, ε_b=4.97%, Group A), followed by severe embrittlement at 8 wt% (ε_b=2.13%, Group D). Conversely, the incorporation of 6 wt% bio-derived SES (PB-SES) completely restored the composite stiffness (E = 1010.74 MPa, Group A) compared to neat PB (951.64 MPa) and exhibited a superior tensile strength (12.09 MPa) compared to its counterpart PB-SE6 (10.20 MPa), at the expense of elongation (ε_b=2.49%). This behaviour suggests that the chemically modified BSG-derived lipid mixture promotes stronger interfacial interactions than the model compound SE, possibly because its broader fatty-acid composition generates a wider distribution of amphiphilic molecules capable of interacting with both the PBS matrix and the BSG surface. In contrast, the epoxidized additives acted predominantly as macromolecular plasticizers, probably due to the high mobility of their oxirane-containing chains. While low EA loadings (2–4 wt%) preserved the baseline stiffness (E = 987–917 MPa, Group A) and tensile strength (σ_b≈15.4–13.9 MPa) of the neat PB, higher concentrations (6–8 wt%) induced a significant softening (down to 728.98 MPa for PB-EA8, Group B), accompanied by a continuous increase in ductility (ε_b=4.66% for PB-EA6). Remarkably, 6 wt% of the bio-based counterpart SEO (PB-SEO) exhibited a Young's modulus (734.78 MPa) and tensile strength (13.62 MPa) statistically equivalent to those of its analogue PB-EA6 but achieved the highest ductility among all tested formulations (ε_b=5.89%, group A), outperforming PB-EA6 by nearly 27%. The contrast between the two bio-derived additives perfectly illustrates how the chemical functionalization dictates the final composite properties: esterification with sucrose (SES) yields a reinforcing agent that maximizes stiffness, whereas epoxidation (SEO) provides a plasticizing effect that maximizes ductility. The superior performance of SES compared with the corresponding model compound SE suggests that the native composition of the BSG lipid fraction contributes positively to interfacial compatibilization. Unlike the model additive synthesized from pure linoleic acid, the BSG-derived product contains a broader distribution of fatty acids together with minor lipidic constituents that may generate a wider range of amphiphilic structures after chemical modification. Such compositional diversity may broaden the spectrum of interactions established at the PBS/BSG interface, promoting more effective adsorption, improved filler wetting and enhanced stress transfer. Although the specific contribution of each component was not investigated in this work, these results indicate that preserving the natural complexity of the biomass may be advantageous rather than detrimental for compatibilizer performance.

According to the literature, interesting information on the compatibilizing effect of an additive can be obtained comparing stress-strain curves of various replicates of a specific sample. A high degree of curve overlap among repeated tensile tests is indicative of uniform mechanical behaviour and effective dispersion of the filler within the matrix (Visco et al., 2024; Watson and Petrie, 2010)

To gain deeper insights into the microstructure and phase homogeneity of the composites, the reproducibility of the stress-strain replicates was systematically evaluated (Figure S45). The neat PB composite exhibited a highly scattered, bimodal fracture behaviour, with several specimens failing prematurely at low strains (1.5–2.0%), indicating that the untreated 30 wt% of BSG filler introduced severe stress-concentration points due to poor wetting and localized agglomeration.

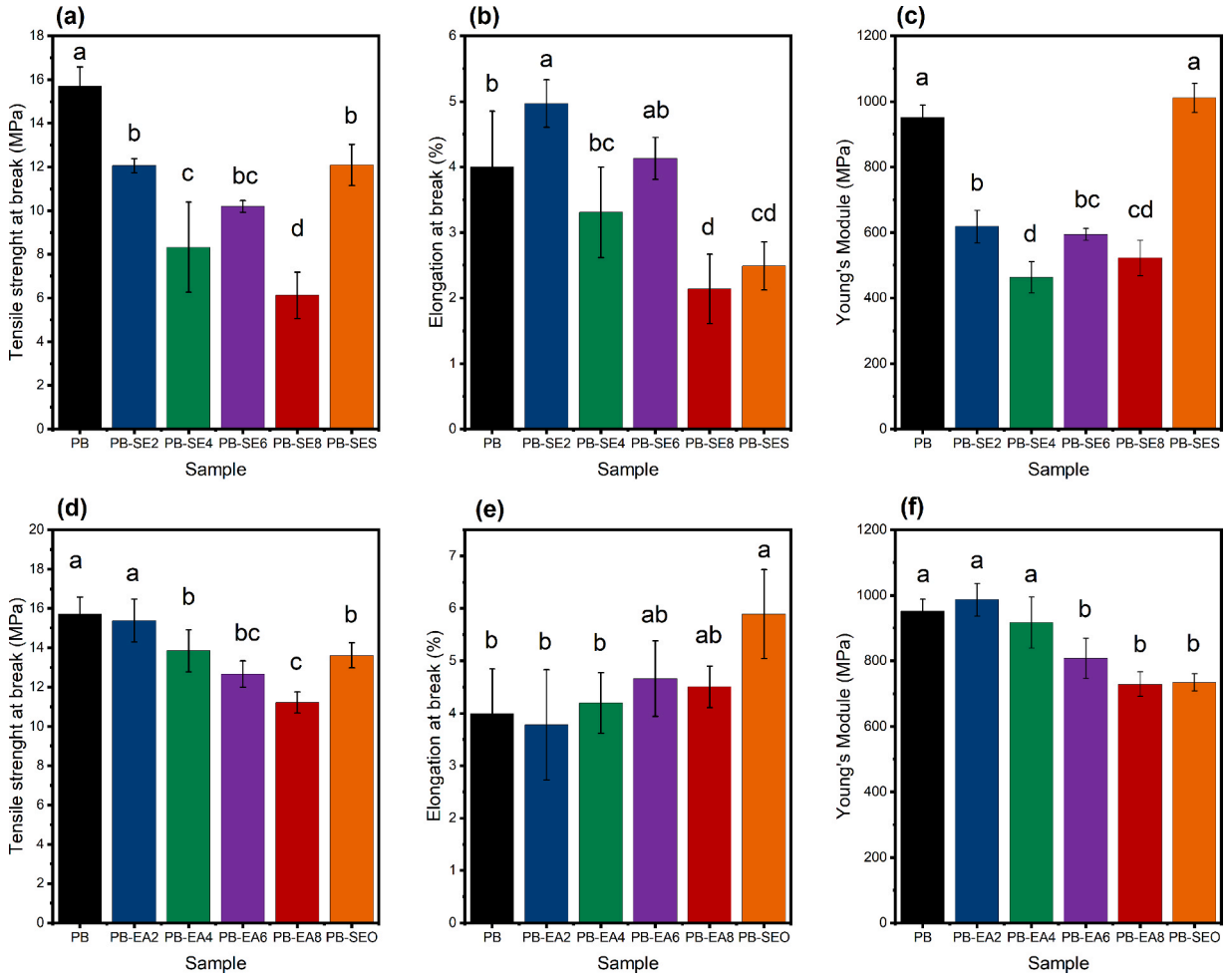

Fig. 2. Tensile strength (MPa), elongation at break (%) and Young's modulus (MPa) of control sample (PB), and formulations containing different wt% of SE and EA (2, 4, 6, 8 wt%) and 6 wt% of BSG-extract-derived SES and SEO (a-f). All tensile tests were performed at room temperature (23 ± 2 °C) and a relative humidity of 50 ± 5% using a crosshead speed of 10 mm/min on standard press-moulded specimens, in compliance with ISO 527 standards. Data are expressed as mean ± standard deviation ($n = 5$). Different letters (a, b, c) above the error bars indicate statistically significant differences ($p < 0.05$) according to one-way ANOVA followed by Tukey's post-hoc test. Statistical comparisons were performed independently for each additive series.

The addition of the sucrose ester (SE) improved curve reproducibility only at the lowest loading (PB-SE2); at higher concentrations (PB-SE4 and PB-SE8), the curves diverged significantly in both stiffness and ductility, suggesting phase separation. In contrast, the bio-derived sucrose ester (PB-SES at 6 wt%) yielded remarkably clustered curves with highly reproducible failure strains (2.2–2.7%), suggesting that its native BSG-derived lipid composition promotes a more uniform coating of the filler and mitigates structural defects. A similar but even more pronounced trend was observed with EA and SEO. While EA led to significant scattering at higher loadings (6–8%) probably due to inefficient interfacial wetting, its bio-based counterpart (PB-SEO) exhibited exceptional curve overlapping. Aside from a single premature failure, the SEO replicates displayed virtually identical elastic slopes and highly consistent plastic deformation regions, failing within a narrow, elevated strain-at-break interval (5.5–7.2%). This outstanding consistency, paired with the fact that SEO achieved the highest overall ductility without compromising tensile strength, confirms that the complex, naturally occurring fatty acid profile of BSG-extracted lipids provides superior lubricating action and higher filler dispersion. Consequently, these results demonstrate that chemical functionalization of BSG lipidic fractions (either via esterification for rigid applications or epoxidation for ductile ones) yields highly compatible biocomposites with structural homogeneity that consistently outperforms their counterparts from linoleic acid.

3.3.2. *Thermal analysis*

All samples were characterized by TGA analysis (see Table 3 and Fig. 3) and data compared with those of PB. For all samples, the first notable weight loss at around 290 °C, is associated with the degradation of BSG, while the second one at around 400 °C corresponds to the degradation of PBS (Fig. 3), in agreement with the literature (Liu et al., 2026; Mainali et al., 2025).

Data show that the addition of increasing wt% of SE or in the presence of 6 wt% SES increased the thermal stability of the biocomposites and residual mass at 600 °C was almost doubled for all samples (Table 3 and Fig. 4). On the contrary, for all PB-EA and PB-SEO specimens, residual values at 600°C were similar or slightly lower than to those of PB (Table 3).

Focusing on the dTG, a notable shift in the decomposition temperature of BSG was observed as the additive loading increased (T_{dpeak}, Table 3 and Fig. 4). Starting from a T_{dpeak} of 295.6 ± 1.1 °C for PB blends, this value increased of up to 318.4 ± 0.6 °C PB-SE8 (~23 °C higher than PB) and to 302.7 ± 3.5 °C for PB-SES. This upward shift, although less pronounced for PB-EA and PB-SEO (Table 3 and Fig. 4), evidences a beneficial effect of the bio-additives on the thermal stability of PBS/BSG composites. The increase in thermal stability observed for the modified composites can be reasonably associated with improved matrix–filler interactions, which are known to limit the exposure of the lignocellulosic phase to thermal degradation (Bellon et al., 2025). Thus,

Table 3
TGA and DSC data.

		TGA			DSC	
Sample	**Residue at 600 °C (%)**	**$T_{d\ peak}$ BSG (°C)**	**$T_{d\ peak}$ PBS (°C)**	**Tm (°C)**	**Tc (°C)**	**χc (%)**
PB	6 ± 0.3^{b}	295.6 ± 1.1^{d}	407.8 ± 0.7^{a}	114.5 ± 0.5^{a}	74.5 ± 0.3^{c}	56.6 ± 5.8^{a}
PB-SE2	12.6 ± 0.7^{a}	307.1 ± 1.7^{bc}	390.3 ± 0.5^{c}	114.2 ± 0.1^{a}	74.5 ± 0.2^{c}	62.2 ± 1.7^{a}
PB-SE4	13.3 ± 1.5^{a}	313.4 ± 3.8^{ab}	388.97 ± 0.51^{cd}	114.08 ± 0.02^{a}	76.2 ± 0.4^{b}	66.9 ± 0.7^{a}
PB-SE6	13.3 ± 2.8^{a}	313.1 ± 1.8^{ab}	387 ± 0.8^{d}	113.7 ± 0.1^{a}	77.1 ± 0.5^{ab}	60.7 ± 4.6^{a}
PB-SE8	16.09 ± 0.03^{a}	318.4 ± 0.6^{a}	388.97 ± 0.3^{cd}	113.8 ± 0.1^{a}	78.5 ± 0.8^{a}	62.9 ± 0.2^{a}
PB-SES	12.4 ± 2.5^{a}	302.7 ± 3.5^{cd}	397.9 ± 1.2^{b}	113.9 ± 0.2^{a}	76.9 ± 0.4^{b}	63.1 ± 1.8^{a}
PB	6 ± 0.3^{a}	295.6 ± 1.1^{b}	407.8 ± 0.7^{a}	114.5 ± 0.5^{a}	74.5 ± 0.3^{a}	56.6 ± 5.8^{a}
PB-EA2	6.1 ± 0.3^{a}	297.8 ± 0.2^{ab}	407.5 ± 0.5^{a}	113.6 ± 0.2^{abc}	74.4 ± 0.3^{a}	63.5 ± 2.8^{a}
PB-EA4	6.2 ± 0.4^{a}	299.3 ± 2.2^{ab}	409 ± 1^{a}	113.8 ± 0.2^{ab}	73 ± 0.2^{abc}	58.6 ± 0.4^{a}
PB-EA6	5.4 ± 0.6^{a}	298.8 ± 1.2^{ab}	407.6 ± 0.2^{a}	113.5 ± 0.2^{bc}	72.5 ± 0.2^{bc}	56.6 ± 0.5^{a}
PB-EA8	6.1 ± 0.4^{a}	300.3 ± 1.2^{a}	406 ± 1^{a}	113.3 ± 0.2^{bc}	71.8 ± 0.1^{c}	56 ± 1^{a}
PB-SEO	5.8 ± 0.6^{a}	297.8 ± 1.2^{ab}	403.4 ± 0.8^{b}	112.9 ± 0.2^{c}	73.7 ± 1.1^{ab}	57.1 ± 3.4^{a}

Residue at 600 °C: residual mass % at 600°C; **T_{dpeak} BSG**: peak temperature of BSG degradation in dTG; **T_{dpeak} PBS**: peak temperature of PBS degradation in dTG; **T_m**: melting temperature; **T_c**: crystallisation temperature; **χ_c**: degree of crystallinity (%). Values within the same column followed by different superscript letters (^{a,b,c}) are statistically different ($p > 0.05$) according to one-way ANOVA followed by Tukey's post-hoc test. Statistical comparisons were performed independently for each additive series

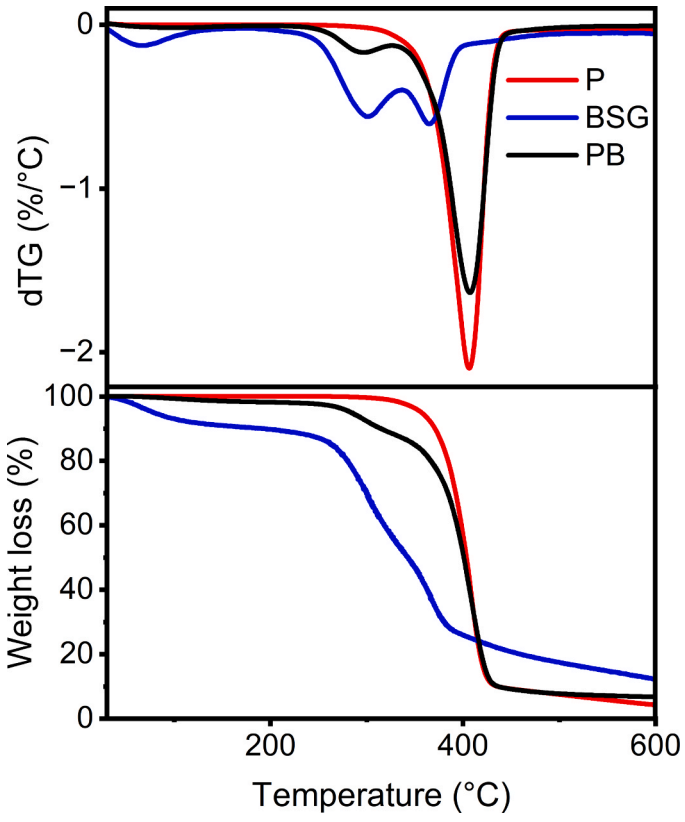

Fig. 3. TGA and dTG profiles of neat PBS (P), neat BSG and the control sample (PB). All tests were conducted under a nitrogen (N_2) atmosphere with a gas flow rate of 20 mL/min, heating from 30 °C to 600 °C at a constant heating rate of 10 °C/min.

increase of T_{dpeak} at higher additive loadings can be attributed to improved interfacial adhesion between the polymer and the filler.

The thermal properties of all specimens prepared were also investigated using Differential Scanning Calorimetry (DSC). Key parameters such as melting temperature (T_m), crystallization temperature (T_c), and degree of crystallinity (χc) were determined. In agreement with the literature, T_m of PB-SE and PB-SES samples remained relatively constant (around 114 °C, $p > 0.05$), and comparable to that of PB (Sin et al., 2013; Turco et al., 2024; Visco et al., 2025), while for PB-EA and PB-SEO a statistically significant decrease was registered, providing clear evidence of a plasticizing effect exerted by EA. On the contrary the crystallization temperature (T_c) of PB-SE specimens showed a significant increase compared to neat PB, reaching a maximum value of about 78 °C for PB-SE6/PB-SE8 (Table 3). These results indicate that the presence of the additive enhances the spatial distribution of BSG within the matrix, acting as a nucleating agent and favouring nucleation phenomena during crystallization (Lathira et al., 2025; Sin et al., 2013). However, regarding the crystallinity degree, the one-way ANOVA test revealed that all formulations belong to the same statistical group (Group A, $p > 0.05$). This indicates that despite minor fluctuations in the mean values, such as the maximum value observed for PB–SE4 ($\chi_c = 66.9\%$), the incorporation of the additives did not induce statistically significant changes in the overall crystalline content compared to neat PB. For PB-EA a gradual decrease in T_c compared to PB was observed as the wt% of EA increased (dropping to 71.8 °C for PB-EA8), further supporting the plasticising effect of EA, which increases chain mobility and hinders the nucleation process. Finally, the T_c and χ_c values of PB-SES were statistically comparable to those of PB-SE4/PB-SE6, while PB-SEO exhibited T_c and χ_c values similar to other PB-EA specimens ($p > 0.05$).

3.3.3. Contact angle

Water contact angle measurements (Fig. 5), performed on the pressmoulded specimen surface, were used to analyse the effect on surface wettability of all samples prepared. PBS exhibited a moderate hydrophobic character with a contact angle of ~70 ° (Hu et al., 2018), and notably the incorporation of 30 wt% BSG (PB) did not substantially alter this value, indicating that the surface properties of the composite are governed both by the polymer matrix and the embedded filler (Visco et al., 2025).

For composites containing SE between 2 and 8 wt%, a decrease in contact angle was observed with additive loading above 6 wt% (Fig. 5). In fact, while PB-SE2 and PB-SE4 formulations showed values close to PB (~65 °), higher concentrations of SE (6 wt% and 8 wt%) drastically reduced wettability resistance, and PB-SE8 showed a very low contact angle (<20 °). This significant reduction suggests that SE strongly increases the biocomposite polarity and hydrophilicity which, in agreement with the literature, can be a consequence of the plasticizing effect of SE, which enhances polymer chain mobility and consequently influences the diffusion process (Carrasco-Guigón et al., 2017). Furthermore, the increase in wettability and hydrophilicity is often correlated with modifications in surface chemistry, particularly the availability of hydroxyl groups on the biocomposite surface, which promote the attraction of water molecules (Remila et al., 2025). PB-SES specimens showed similar contact angles to PB-SE2 and PB-SE4 (~65 °), although significantly improved compared to that of PB-SE6 (Fig. 5).

At lower EA loadings (2–4 wt%), PB-EA composites (Fig. 5) exhibited contact angles comparable to those of the PB, PB-SE2, and PB-SE4 samples. It is worth noting that, with quantities of EA above 6 wt%, a marked increase in hydrophobicity was registered, reaching ~80 ° for PB-EA6 and ~85 ° for PB-EA8. The observed increase in contact angle reflects a reduction in surface wettability, suggesting that the additive effectively masks hydrophilic domains at the composite surface due to the formation of low energy interactions (for example Hydrogen bonds,

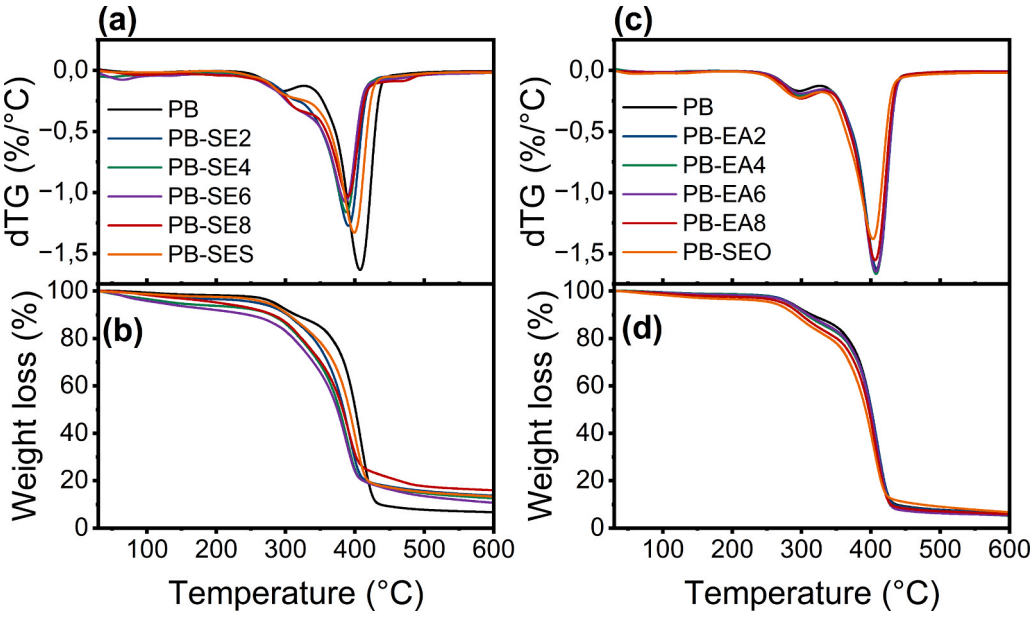

Fig. 4. (a) TGA and (b) dTG profiles of composites containing SE and SES; **(c)** TGA and **(d)** DTG profiles of composites containing EA and SEO. The control sample (PB) is represented by the black solid line. All tests were conducted under a nitrogen (N_2) atmosphere with a gas flow rate of 20 mL/min, heating from 30 °C to 600 °C at a constant heating rate of 10 °C/min.

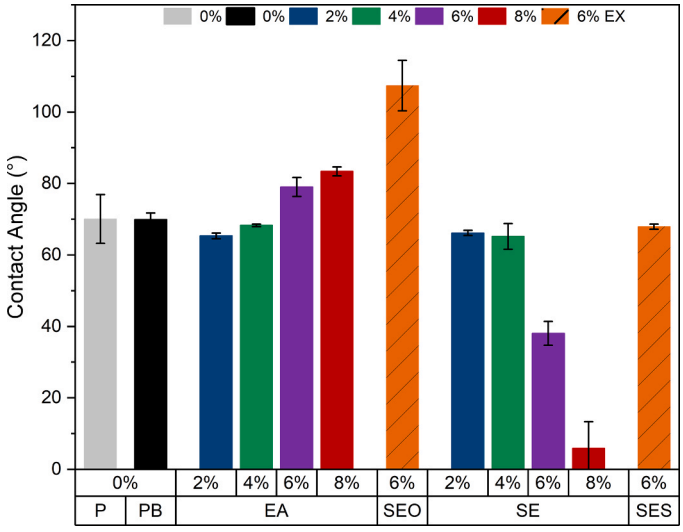

Fig. 5. Water contact angle (WCA) of PB containing SE and EA (0–8 wt%, solid bars) and PB containing 6 wt% SES and SEO (patterned bars). Measurements were performed on specimen surfaces after 10 s using a 10 μL deionized water droplet (Celeston microscope, ImageJ software). Data represent the mean ± standard deviation of three replicates.

Van Der Waals interactions), reducing the biocomposites overall water affinity and consequently improving PB-EA6 and PB-EA8 hydrophobicity. BC prepared with epoxidized BSG derived additives (PB-SEO) showed the highest contact angle values (> 100 °), indicating a significant improvement in hydrophobicity, significantly higher than the pristine polymer, PBS/BSG composites and among the highest reported in the literature both for reactive and non-reactive biocomposites formulations (Barrino et al., 2023; Gaidukovs et al., 2022; Hassaini et al., 2016; Soccio et al., 2020). This improvement may possibly be attributed to the presence of 18% of saturated stearic acid in the BSG extract compared to linoleic acid which increases the hydrophobicity of SEO.

3.3.4. ATR and SEM analysis

ATR-FTIR of PB-SE, PB-EA, PB-SES and PB-SEO samples are reported in Fig. 6. The region of interest is located around 1715 cm^{-1} and is attributed to the stretching vibration of the carbonyl group of PBS. Shifts in this band are significant for evaluating whether interactions between the matrix and the filler have formed within the biocomposite, potentially mediated by the presence of the additive. A shift to lower wavenumbers (redshift) is associated with an increase in such interactions, weakening the carbonyl bond due to these newly established interactions, which lower the energy required for vibrational excitation (Ahmed et al., 2018).

In both diagrams of Fig. 6, a redshift of the carbonyl peak is observed for all formulations as compared to PB (black line). This shift suggests the formation of interactions of different magnitude between P and BSG, most likely hydrogen bonding or dipole–dipole interactions, promoted by the bio-additives. For instance, in Fig. 6a, the carbonyl band shifts from 1717.6 ± 0.3 cm^{-1} (PB, black line) to 1712.7 ± 0.9 cm^{-1} and 1714.7 ± 0.7 for cm^{-1} PB-SE2/PB-SES, probably due to the presence of interfacial interactions within the biocomposites. Similar considerations apply for Fig. 6b (PE-EA and PE-SEO composites).

To complement the mechanical, thermal, and spectroscopic analyses, the fracture surfaces of the composites were examined by scanning electron microscopy (SEM). Morphological observations provide direct information on the dispersion of the BSG particles within the PBS matrix and on the quality of the matrix–filler interface, allowing the compatibilizing effect of the bio-based additives inferred from the previous analyses to be visually assessed.

SEM micrographs of dumbbell samples after fracture tests are reported in Fig. 7. PB exhibits a rough and heterogeneous fracture surface, and the morphology reveals poor interfacial adhesion between the polymer matrix and the filler particles. The presence of voids and detached filler domains within the fracture surface reflects limited stress transfer between PBS and BSG, consistent with weak interfacial bonding.

In contrast, the addition of SE leads to a noticeable change in the fracture surface morphology. The fracture surface of the PB-SE6 sample is considerably denser and more uniform. Evidence of particle pull-out is minimal, and the filler particles are more tightly surrounded by the PBS matrix. This suggests that SE effectively improves the interfacial

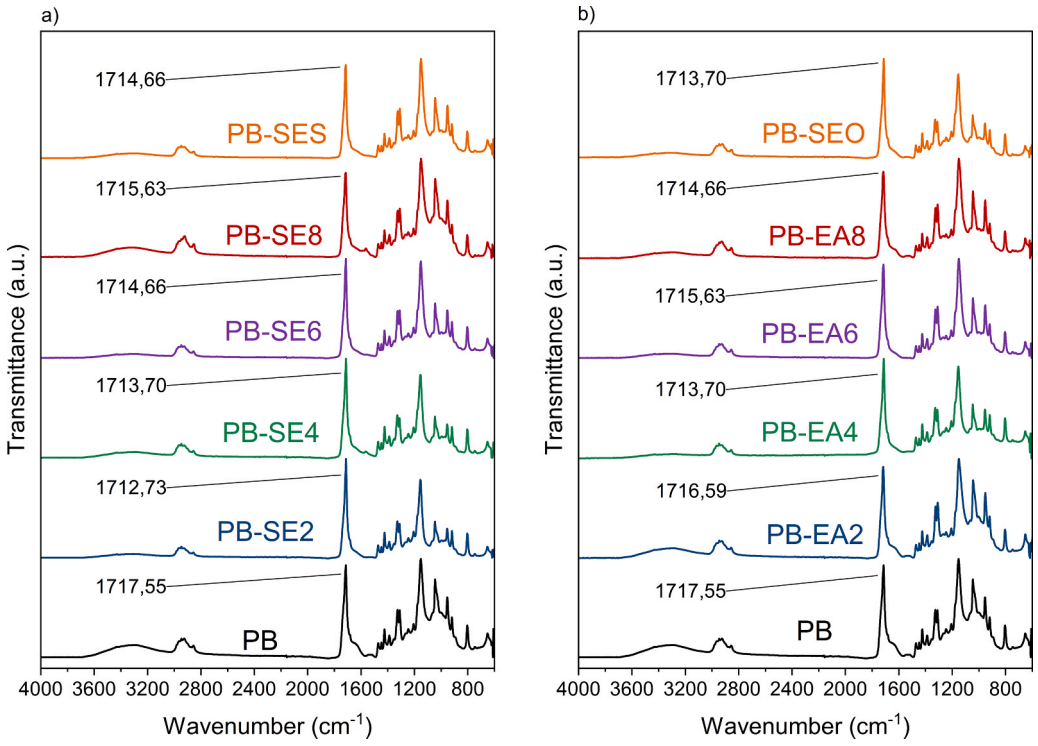

Fig. 6. Comparison of normalized ATR-FTIR spectra (4000 – 400cm^{-1}) recorded on specimen surfaces of a) PB containing 0–8 wt% SE and 6 wt% SES and b) PB containing 0–8 wt% EA and 6 wt% SEO. Spectra were normalized (Min-Max) using PerkinElmer Spectrum software.

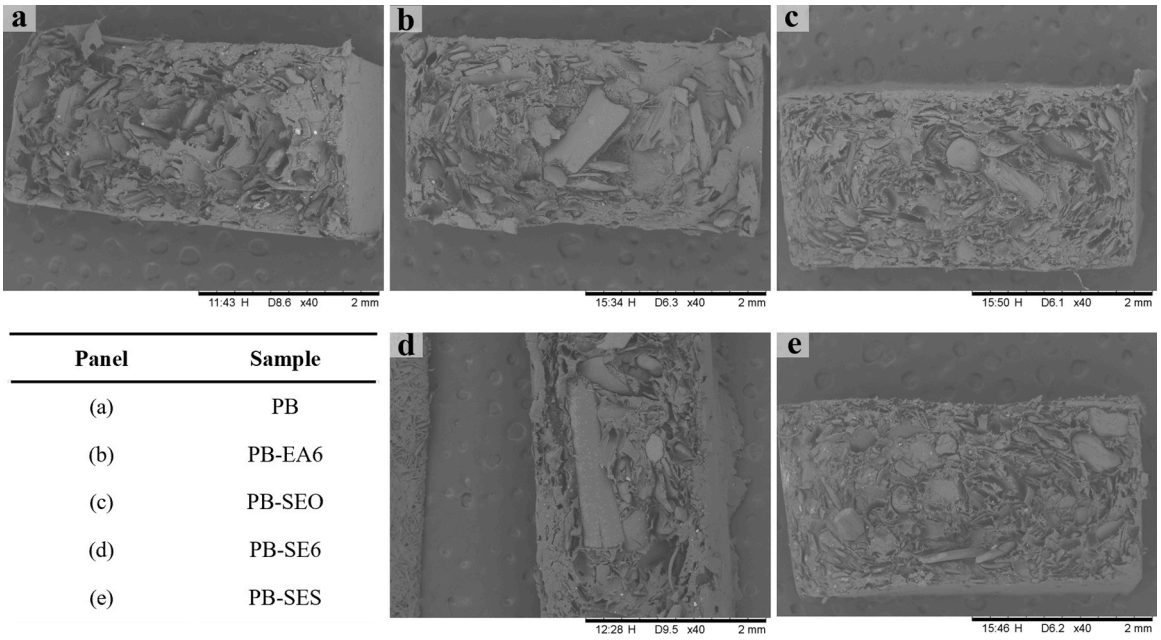

Panel	Sample
(a)	PB
(b)	PB-EA6
(c)	PB-SEO
(d)	PB-SE6
(e)	PB-SES

Fig. 7. SEM micrographs (40 × magnification) of the fracture surfaces of a) PB, b-c) PB containing 6 wt% EA and 6 wt% SEO and d-e) PB containing 6 wt% SE and 6 wt% SES. Prior to analysis, the dumbbell-shaped specimens were gold-coated using a K450X sputter coater. Micrographs were recorded using a Hitachi TM3000 scanning electron microscope operating at an accelerating voltage of 5.0 kV. Scale bars represent 2 mm.

adhesion between P and BSG, facilitating a more cohesive stress transfer during mechanical testing. Analogous considerations apply for bio-composites prepared in the presence of SES. The observed transition from a brittle, non-cohesive fracture surface in PB to a denser, more cohesive morphology with increasing additive concentration confirms that SE and SES successfully enhance the interfacial adhesion, thereby improving the overall compatibility of the components.

On the other hand, SEM analysis of PB-EA6 sample reveals a morphology that is only marginally less refined than that of the PB-SE6, remaining largely comparable to the results reported above. Most notably, PB-SEO exhibits a morphology closely paralleling that of PB-SES which is consistent with an effective compatibilizing action.

Overall, the combined mechanical, thermal, spectroscopic and morphological results consistently indicate that sucrose esters derived

from BSG lipids effectively improve the compatibility between PBS and BSG. Interestingly, the BSG-derived compatibilizers did not simply reproduce the behaviour of the model additives but, in several cases, outperformed them. This finding suggests that the intrinsic molecular complexity of the lipid fraction, generally regarded as a disadvantage for chemical valorisation, may instead represent an advantage by generating a broader population of amphiphilic molecules capable of interacting with both the polymer matrix and the lignocellulosic filler.

3.3.5. Biocomposites Colour analysis

Colorimetric parameters of all specimens (L*, a*, b*, ΔE) and browning index (BI), Chroma and Hue are summarized in Table 4. As expected, the incorporation of BSG strongly reduces the brightness (L*) of the composites compared to the pure polymer (L* = 80.48), with values ranging between 43.64 and 51.80, depending on the formulation. Although the origin of colour variations cannot be unequivocally established, since they may arise from modifications of the BSG filler, the PBS matrix or melt processing conditions, in agreement with the literature (Visco et al., 2026), PB showed L* = 47.31, confirming the strong darkening effect imparted by the lignocellulosic filler. Additives slightly reduce this effect and in fact PB-SE6 and PB-SE8 exhibited somewhat higher L* values (51.80 and 50.80, respectively), suggesting a partial mitigation of the darkening effect of BSG. Conversely, PB-SES and PB-SEO displayed the lowest brightness (L* = 44.16 and 43.64), probably due to the fact that these compatibilizers enhance filler dispersion in the matrix that intensify the overall dark colour. Data indicate that the presence of increasing quantities of SE and EA slightly modulate brightness, while the darkening effect of BSG remains dominant.

Moreover, the best morphological improvements observed by SEM analysis (see above) can be correlated with the strongest reduction in brightness and highest ΔE, suggesting that enhanced matrix–filler adhesion may also increase light absorption and colour homogeneity in the composites (Petaloti et al., 2025).

3.3.6. Biofragmentation

The biofragmentation behaviour of best performing biocomposite formulations was monitored up to 180 days under controlled soil conditions (Fig. 8, Table S 2), according to a standard procedure reported in the literature (Santandrea et al., 2026). All formulations exhibited a gradual decrease in weight over time, although the degradation rate strongly depended on the type and amount of additive used. Reference composite (PB) mass loss was rather low, reaching approximately 16 wt % after 180 days. Analogously, PB-SE4/PE-SE6 and PB-SES showed a moderate mass loss (between 11 and 22 wt%). A more pronounced effect was observed for the EA-based composites (Fig. 8 and Table S 2), and PB-EA6 exhibited the highest degradation rate, losing about 80 wt% of its initial mass after 182 days. This can be possibly attributed to the higher heterogeneous structure of PB-EA composites, allowing for a quicker microbial diffusion and degradation. Conversely, PB-SEO showed intermediate behaviour, degrading more slowly compared to PB-EA6 (26.08%), but still faster than PB. Overall, these trends align with previous observations on polyester-based biocomposites containing agro-industrial residues, where lignocellulosic fillers and lipid-derived additives accelerate biodegradation by increasing hydrophilicity and promoting microbial colonisation (Gaidukova et al., 2021).

4. Conclusions

The present study demonstrates the dual role of Brewer's Spent Grain (BSG) both as a valuable source of lipids for bio-based additives and sustainable bio-filler for the production of PBS-based biocomposites. The extraction of the lipid fraction from BSG and its subsequent chemical modification into sucrose esters (SES) and epoxidized derivatives (SEO) provides an effective, non-toxic alternative to conventional fossil-based additives. The synthesized bio-additives (SE, EA) and their BSG-derived counterparts (SES, SEO) influenced the properties of PBS/BSG biocomposites through two distinct mechanisms. Structurally, both series significantly enhanced thermal stability: the degradation

Table 4
Values of *L**, *a** and *b**, BI, chroma, hue and total colour difference (ΔE) of PBS, PB, and PB-SE, PB-EA, PB-SES, PB-SEO.

Sample	L*	a*	b*	BI	Chroma	Hue	ΔE	Pseudo color D65
PBS	80.48±0.53	0.05±0.01	5.19±1.89	0.68	5.19	1.56		
PB	47.31±0.49	5.84±0.49	17.11±0.16	12.37	18.08	1.24	35.72	
PB-SE2	48.25±1.17	5.72±0.59	17.76±0.29	12.09	18.66	1.25	35.06	
PB-SE4	47.60±0.37	6.61±0.05	18.77±0.01	13.77	19.90	1.23	36.17	
PB-SE6	51.8±0.89	6.16±0.08	18.52±0.31	12.01	19.52	1.24	32.21	
PB-SE8	50.80±1.2	6.61±0.42	20.31±1.88	13.22	21.36	1.25	33.95	
PB-EA2	47.26±0.83	6.45±0.18	18.19±0.18	13.51	19.29	1.23	36.24	
PB-EA4	47.21±0.52	6.54±0.05	17.61±0.18	13.54	18.79	1.21	36.10	
PB-EA6	46.93±0.68	6.49±0.07	18.02±0.14	13.63	19.15	1.22	36.49	
PB-EA8	48.36±0.82	6.09±0.15	16.49±0.51	12.32	17.58	1.21	34.58	
PB-SES	44.16±0.38	6.78±0.19	17.44±0.27	14.79	18.71	1.20	38.92	
PB-SEO	43.64±0.73	6.45±0.13	15.67±0.69	14.03	16.95	1.18	38.83	

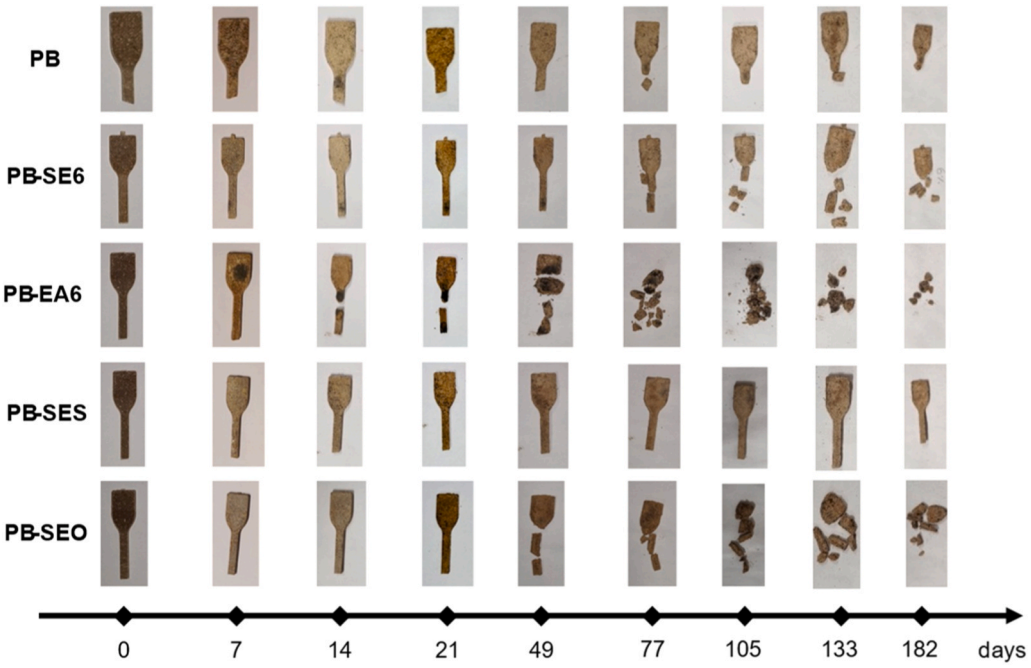

Fig. 8. Visual evaluation of the biofragmentation of biocomposite dumbbell-shaped specimens during burial tests in soil at predetermined time intervals up to 182 days. The panel compares control sample (**PB**) with formulations containing 6 wt% SE (**PB-SE6**), EA (**PB-EA6**), and 6 wt% SES and SEO (**PB-SES** and **PB-SEO**). Samples were buried in soil under controlled temperature and humidity according to literature procedures (Piñeros-Hernandez et al., 2017b).

temperature of the BSG component ($T_{d\ \mathrm{peak}}$ BSG) shifted systematically toward higher values, registering increases from + 8 °C up to + 23 °C compared to the neat PB. This stabilization successfully widens the processing window, ensuring safe margins for industrial injection moulding. However, a clear divergence emerged in their governing mechanisms. SE and SES explicitly acted as heterogeneous nucleating agents, accelerating matrix crystallization (T_c increasing up to 78.5 °C). Conversely, the EA series and SEO functioned predominantly as plasticizers, as consistently evidenced by the systematic depression of thermal transitions (T_m and T_c) and the cross-validated tensile mechanical behavior

Furthermore, the additives significantly influenced the environmental profile of the composites: the PB-EA4/PB-EA6 formulations showed a remarkable acceleration in soil biodegradation, reaching a mass loss of approximately 50 and 80 wt% respectively, after 182 days. These results prove that the addition of SE, EA, SES, and SEO to the biocomposites allows for improved thermal stability of the BSG component, while simultaneously enhancing its overall circularity. This concept may be extended to other agro-industrial residues containing recoverable lipid fractions, opening new opportunities for the design of fully bio-based composite systems.

Future research will focus on further optimizing this circular model. Specifically, studies are underway to evaluate the performance of extracted BSG (the residue remaining after lipid extraction) as a filler, comparing its reinforcing capabilities with those of virgin BSG. Additionally, future efforts will aim to extract cellulose directly from the spent grain to serve as a platform for chemical modification, potentially leading to a new generation of fully BSG-derived bio-additives and further reducing reliance on external raw materials.

Beyond demonstrating the compatibilizing effect of the synthesized additives, this work introduces an integrated approach for the utilization of brewer's spent grain, in which two chemically distinct fractions are exploited for complementary functions within the same material. While the lignocellulosic fraction provides structural reinforcement, the lipid fraction is chemically upgraded into functional compatibilizers capable of improving interfacial adhesion. This strategy extends the role of BSG from a passive bio-filler to a multifunctional feedstock for composite manufacturing, thereby increasing the value extracted from a single agricultural residue while reducing the reliance on fossil-derived additives.

CRediT authorship contribution statement

Gioele Foltran: Writing – review & editing, Writing – original draft, Methodology, Investigation, Formal analysis, Data curation. **Valentina Beghetto:** Writing – review & editing, Writing – original draft, Methodology, Funding acquisition, Formal analysis, Data curation, Conceptualization. **Silvia Conca:** Writing – review & editing, Investigation, Data curation.

Funding

National Recovery and Resilience Plan (PNRR), for the 40th PhD cycle "National Interest PhD Program in Design for Made in Italy: Identity, Innovation, and Sustainability, administrative headquarter University of Campania "Luigi Vanvitelli", Caserta (Italy)

Declaration of Competing Interest

The authors declare that they have no known competing financial interests or personal relationships that could have appeared to influence the work reported in this paper.

Acknowledgments

The Authors would like to express their sincere gratitude to Dr. Noemi Bardella for her mentorship at the beginning of this project, which was instrumental in clarifying the principles of thermal characterization and NMR spectroscopy

Appendix A. Supporting information

Supplementary data associated with this article can be found in the online version at doi:10.1016/j.indcrop.2026.124135.

Data availability

Data will be made available on request.

References

Ahmed, I., Niazi, M.B.K., Hussain, A., Jahan, Z., 2018. Influence of amphiphilic plasticizer on properties of thermoplastic starch films. Polym. Plast. Technol. Eng. 57, 17–27. https://doi.org/10.1080/03602559.2017.1298803.

Allouzi, M.M.A., Tang, D.Y.Y., Chew, K.W., Rinklebe, J., Bolan, N., Allouzi, S.M.A., Show, P.L., 2021. Micro (nano) plastic pollution: the ecological influence on soil-plant system and human health. Sci. Total. Environ. 788, 147815. https://doi.org/10.1016/j.scitotenv.2021.147815.

Baiano, A., Fiore, A., 2025. Development and characterization of brewers' spent grain-based materials. Circ. Econ. 4, 100158. https://doi.org/10.1016/j.cec.2025.100158.

Bardella, N., Facchin, M., Fabris, E., Baldan, M., Beghetto, V., 2024. Waste Cooking Oil as Eco-Friendly Rejuvenator for Reclaimed Asphalt Pavement. Materials 17, 1477. https://doi.org/10.3390/ma17071477.

Barrino, F., De La Rosa-Ramírez, H., Schiraldi, C., López-Martínez, J., Samper, M.D., 2023. Preparation and Characterization of New Bioplastics Based on Polybutylene Succinate (PBS). Polymers 15, 1212. https://doi.org/10.3390/polym15051212.

Beghetto, V., 2025a. Strategies for the Transformation of Waste Cooking Oils into High-Value Products: A Critical Review. Polymers 17, 368. https://doi.org/10.3390/polym17030368.

Beghetto, V., 2025b. Waste Cooking Oils into High-Value Products: Where Is the Industry Going? Polymers 17, 887. https://doi.org/10.3390/polym17070887.

Beghetto, V., Conca, S., Santandrea, D., 2026. Carboxymethyl Cellulose-Based Films for Sustainable Food Packaging: Modification Strategies and Structure–Property Relationships. Polymers 18, 552. https://doi.org/10.3390/polym18050552.

Beghetto, V., Gatto, V., Samiolo, R., Scolaro, C., Brahimi, S., Facchin, M., Visco, A., 2023. Plastics today: Key challenges and EU strategies towards carbon neutrality: A review. Environ. Pollut. 334, 122102. https://doi.org/10.1016/j.envpol.2023.122102.

Belardi, I., Sarasini, F., Tirillò, J., Russo, P., De Francesco, G., Marconi, O., Marrocchi, A., 2025. Brewers' Spent Grain-Derived Arabinoxylan as a Sustainable Filler for Enhanced PHBV Biocomposites. Polymers 17, 114. https://doi.org/10.3390/polym17010114.

Bellon, J., Bacoup, F., Marais, S., Gattin, R., 2025. PLA, PBS, and PBAT Biocomposites—Part A: Matrix–Filler Interactions with Agro-Industrial Waste Fillers (Brewer's Spent Grain, Orange Peel) and Their Influence on Thermal, Mechanical, and Water Sorption Properties. Materials 18, 3867. https://doi.org/10.3390/ma18163867.

Canzian, N., Foltran, G., Beghetto, V., 2026. Turning unsorted stranded seaweeds into biocomposites. Mater. Today Commun. 52, 115228. https://doi.org/10.1016/j.mtcomm.2026.115228.

Carrasco-Guigón, F., Rodríguez-Félix, D., Castillo-Ortega, M., Santacruz-Ortega, H., Burruel-Ibarra, S., Encinas-Encinas, J., Plascencia-Jatomea, M., Herrera-Franco, P., Madera-Santana, T., 2017. Preparation and Characterization of Extruded Composites Based on Polypropylene and Chitosan Compatibilized with Polypropylene-Graft-Maleic Anhydride. Materials 10, 105. https://doi.org/10.3390/ma10020105.

Chandran, M., Tamilkolundu, S., Murugesan, C., 2020. Conversion of plastic waste to fuel. in: Plastic Waste and Recycling. Elsevier, pp. 385–399. https://doi.org/10.1016/B978-0-12-817880-5.00014-1.

Chinn, A.F., Trindade Coutinho, I., Kethireddy, S.R., Williams, N.R., Knott, K.M., Moore, R.B., Matson, J.B., 2024. Ethyl cellulose- *block* -poly(benzyl glutamate) block copolymer compatibilizers for ethyl cellulose/poly(ethylene terephthalate) blends. Polym. Chem. 15, 3501–3509. https://doi.org/10.1039/D4PY00688G.

Choo, J.E., Park, T.H., Jeon, S.M., Hwang, S.W., 2023. The Effect of Epoxidized Soybean Oil on the Physical and Mechanical Properties of PLA/PBAT/PPC Blends by the Reactive Compatibilization. J. Polym. Environ. 31, 4007–4021. https://doi.org/10.1007/s10924-023-02862-6.

Coppola, G., Gaudio, M.T., Lopresto, C.G., Calabro, V., Curcio, S., Chakraborty, S., 2021. Bioplastic from Renewable Biomass: A Facile Solution for a Greener Environment. Earth Syst. Environ. 5, 231–251. https://doi.org/10.1007/s41748-021-00208-7.

Del Río, J.C., Prinsen, P., Gutiérrez, A., 2013. Chemical composition of lipids in brewer's spent grain: A promising source of valuable phytochemicals. J. Cereal Sci. 58, 248–254. https://doi.org/10.1016/j.jcs.2013.07.001.

Dominguez-Candela, I., Gomez-Caturla, J., Cardona, S.C., Lora-García, J., Fombuena, V., 2022. Novel compatibilizers and plasticizers developed from epoxidized and maleinized chia oil in composites based on PLA and chia seed flour. Eur. Polym. J. 173, 111289. https://doi.org/10.1016/j.eurpolymj.2022.111289.

Dutta, N., Bhadra, B., Gogoi, G., Kumar Maji, T., 2021. Development of polyvinyl chloride/waste rice husk ash/modified montmorillonite nanocomposite using epoxidized soybean oil as green additive substituting synthetic plasticizer and compatibiliser. Clean. Mater. 2, 100033. https://doi.org/10.1016/j.clema.2021.100033.

Environment, U.N, 2021. Drowning in Plastics – Marine Litter and Plastic Waste Vital Graphics | UNEP - UN Environment Programme [WWW Document]. URL https://www.unep.org/resources/report/drowning-plastics-marine-litter-and-plastic-waste-vital-graphics (accessed 9.24.25).

European Bioplastics, 2024. Bioplastics Market Development Update 2024, Market Data Report. Berlin.

Faheem, M., Khan, K.A., 2025. Harnessing sustainable biocomposites: a review of advances in greener materials and manufacturing strategies. Polym. Bull. https://doi.org/10.1007/s00289-025-05916-y.

Fang, Y.-G., Lin, J.-Y., Zhang, Y.-C., Qiu, Q.-W., Zeng, Y., Li, W.-X., Wang, Z.-Y., 2024. A reactive compatibilization with the compound containing four epoxy groups for polylactic acid/poly(butylene adipate-co-terephthalate)/thermoplastic starch ternary bio-composites. Int. J. Biol. Macromol. 262, 129998. https://doi.org/10.1016/j.ijbiomac.2024.129998.

Ferrentino, G., Ndayishimiye, J., Haman, N., Scampicchio, M., 2019. Functional Activity of Oils from Brewer's Spent Grain Extracted by Supercritical Carbon Dioxide. Food Bioprocess. Technol. 12, 789–798. https://doi.org/10.1007/s11947-019-02249-3.

Fong, M.N.F., Salimon, J., 2012. Epoxidation of Palm Kernel Oil Fatty Acids. J. Sci. Technol. 4, 87–97.

Fredi, G., Dorigato, A., 2024. Compatibilization of biopolymer blends: A review. Adv. Ind. Eng. Polym. Res. 7, 373–404. https://doi.org/10.1016/j.aiepr.2023.11.002.

Gaidukova, G., Platnieks, O., Aunins, A., Barkane, A., Ingrao, C., Gaidukovs, S., 2021. Spent coffee waste as a renewable source for the production of sustainable poly (butylene succinate) biocomposites from a circular economy perspective. RSC Adv. 11, 18580–18589. https://doi.org/10.1039/D1RA03203H.

Gaidukovs, S., Platnieks, O., Gaidukova, G., Starkova, O., Barkane, A., Beluns, S., Thakur, V.K., 2022. Understanding the Impact of Microcrystalline Cellulose Modification on Durability and Biodegradation of Highly Loaded Biocomposites for Woody Like Materials Applications. J. Polym. Environ. 30, 1435–1450. https://doi.org/10.1007/s10924-021-02291-3.

Grand View Research, 2024. Bioplastics Market Size, Share, Growth Analysis Report 2030. Grand View Research, San Francisco.

Guillén, M.D., Ruiz, A., 2003. Rapid simultaneous determination by proton NMR of unsaturation and composition of acyl groups in vegetable oils. Eur. J. Lipid Sci. Technol. 105, 688–696. https://doi.org/10.1002/ejlt.200300866.

Hassaini, L., Kaci, M., Benhamida, A., Bruzaud, S., Pillin, I., Grohens, Y., 2016. The effects of PHBV- *g* -MA compatibilizer on morphology and properties of poly(3-hydroxybutyrate-Co-3-hydroxyvalerate)/olive husk flour composites. J. Adhes. Sci. Technol. 30, 2061–2080. https://doi.org/10.1080/01694243.2016.1168961.

Hejna, A., Barczewski, M., Kosmela, P., Mysiukiewicz, O., 2025. Structure, performance, and photooxidative stability of Mater-Bi/brewers' spent grain composites as a function of filler thermomechanical and chemical modification. Ind. Crops Prod. 224, 120421. https://doi.org/10.1016/j.indcrop.2024.120421.

Hejna, A., Waliszewska, B., Zborowska, M., Barczewski, M., Szulc, J., Paszkot, J., Kawa-Rygielska, J., Kosmela, P., Woźniak, M., Ratajczak, I., Piasecki, A., Cygan, T., Sałasińska, K., 2026. Deepening the understanding and extending the potential of waste biomass temperature treatment using sunflower husk as an example. Biomass-.-. Bioenergy 207, 108718. https://doi.org/10.1016/j.biombioe.2025.108718.

Henkin, J.M., Mainali, K., Sharma, B.K., Yadav, M.P., Ngo, H., Sarker, M.I., 2025. A Review of Chemical and Physical Analysis, Processing, and Repurposing of Brewers' Spent Grain. Biomass 5, 42. https://doi.org/10.3390/biomass5030042.

Hu, X., Su, T., Li, P., Wang, Z., 2018. Blending modification of PBS/PLA and its enzymatic degradation. Polym. Bull. 75, 533–546. https://doi.org/10.1007/s00289-017-2054-7.

Imre, B., Pukánszky, B., 2013. Compatibilization in bio-based and biodegradable polymer blends. Eur. Polym. J. 49, 1215–1233. https://doi.org/10.1016/j.eurpolymj.2013.01.019.

Imre, B., García, L., Puglia, D., Vilaplana, F., 2019. Reactive compatibilization of plant polysaccharides and biobased polymers: Review on current strategies, expectations and reality. Carbohydr. Polym. 209, 20–37. https://doi.org/10.1016/j.carbpol.2018.12.082.

Intranuwong, J., Nongyai, N., Shin, S.K., Kim, M., Kwon, Y.K., 2025. Effect of Epoxidized Soybean Oil on Biodegradation and Mechanical Performances of Thermoplastic Starch/Poly(Butylene Adipate-Co-Terephthalate). J. Appl. Polym. Sci. 142, e57401. https://doi.org/10.1002/app.57401.

Jambeck, J.R., Geyer, R., Wilcox, C., Siegler, T.R., Perryman, M., Andrady, A., Narayan, R., Law, K.L., 2015. Plastic waste inputs from land into the ocean. Science 347, 768–771. https://doi.org/10.1126/science.1260352.

Jeepery, I.F., Goto, T., Sudesh, K., Abe, H., 2023. Biodegradable block copolymer as compatibilizer and blend component of poly(3-hydroxybutyrate-co-3-hydroxyhexanoate)-based polyester blends. Eur. Polym. J. 196, 112314. https://doi.org/10.1016/j.eurpolymj.2023.112314.

Kavalopoulos, M., Stoumpou, V., Christofi, A., Mai, S., Barampouti, E.M., Moustakas, K., Malamis, D., Loizidou, M., 2021. Sustainable valorisation pathways mitigating environmental pollution from brewers' spent grains. Environ. Pollut. 270, 116069. https://doi.org/10.1016/j.envpol.2020.116069.

Lackner, M., Besharati, M., 2025. Agricultural Waste: Challenges and Solutions, a Review. Waste 3, 18. https://doi.org/10.3390/waste3020018.

Lathira, G., Klonos, P.A., Xanthopoulou, E., Tsachouridis, K., Kyritsis, A., Valera Gómez, M.Á., Mangas, A., Albaladejo, P., Sánchez, R., Bikiaris, D.N., Terzopoulou, Z., 2025. Improving the performance of poly(lactic acid)/ POLY(BUTYLENE SUCCINATE) blends by compatibilization and reinforcement with nanofibrillated cellulose. Polym. Eng. Sci. 65, 3114–3133. https://doi.org/10.1002/pen.27203.

Latos-Brozio, M., Rułka, K., Masek, A., 2025. Review of Bio-Fillers Dedicated to Polymer Compositions. Chem. Biodivers. 22, e202500406. https://doi.org/10.1002/cbdv.202500406.

Lisci, S., Tronci, S., Grosso, M., Hajrizaj, R., Sibono, L., Karring, H., Gerganov, A., Maschietti, M., Errico, M., 2024. Valorizing brewer's spent grain: A sequential pathway of supercritical extraction, hydrolysis, and fermentation. Chem. Eng. Sci. 285, 119620. https://doi.org/10.1016/j.ces.2023.119620.

Liu, P., Sun, S., Li, X., Huang, S., Wu, Y., Li, Z., Wei, X., Wu, S., 2026. A comprehensive study on pyrolysis behavior and product characteristic of different components in brewer's spent grains. Fuel 406, 136749. https://doi.org/10.1016/j.fuel.2025.136749.

Ma, Z., Yin, T., Jiang, Z., Weng, Y., Zhang, C., 2024. Bio-based epoxidized soybean oil branched cardanol ethers as compatibilizers of polybutylene succinate (PBS)/polyglycolic acid (PGA) blends. Int. J. Biol. Macromol. 259, 129319. https://doi.org/10.1016/j.ijbiomac.2024.129319.

Mainali, K., Sarker, M.I., Sharma, B.K., Ellison, C., Ngo, H., Simon, S., Yadav, M.P., 2025. Thermal, Rheological, and Surface Properties of Brewer's Spent Grain and Its Oligo and Polysaccharides Fractions. Foods 14, 4170. https://doi.org/10.3390/foods14244170.

Manu, T., Nazmi, A.R., Shahri, B., Emerson, N., Huber, T., 2022. Biocomposites: A review of materials and perception. Mater. Today Commun. 31, 103308. https://doi.org/10.1016/j.mtcomm.2022.103308.

MarketsandMarkets, 2025. Biodegradable Plastic Additives Market by Chemistry Type (Bio-based Aromatic, Bio-based Non-aromatic), Type (Bio-based Plasticizers, Bio-based Stabilizers, Bio-based Flame Retardants), End-use Industry, and Region - Global Forecast to 2030 (No. CH 8205). MarketsandMarkets.

Nayanathara Thathsarani Pilapitiya, P.G.C., Ratnayake, A.S., 2024. The world of plastic waste: A review. Clean. Mater. 11, 100220. https://doi.org/10.1016/j.clema.2024.100220.

Olonisakin, K., Mohanty, A.K., Thimmanagari, M., Misra, M., 2025. Recent advances in biodegradable polymer blends and their biocomposites: a comprehensive review. Green. Chem. 27, 11656–11704. https://doi.org/10.1039/D5GC01294E.

Pęśko, M., Masek, A., 2025. Plant-Based Biofillers for Polymer Composites: Characterization, Surface Modification, and Application Potential. Polymers 17, 2286. https://doi.org/10.3390/polym17172286.

Petaloti, A.-I., Paraskevopoulou, A., Achilias, D.S., 2025. Preparation and Characterization of Biocomposite Films with Enhanced Oxygen Barrier and Antioxidant Properties Based on Polylactide and Extracts from Coffee Silverskin. Molecules 30, 1383. https://doi.org/10.3390/molecules30061383.

Phua, Y.J., Lau, N.S., Sudesh, K., Chow, W.S., Mohd Ishak, Z.A., 2012. Biodegradability studies of poly(butylene succinate)/organo-montmorillonite nanocomposites under controlled compost soil conditions: Effects of clay loading and compatibiliser. Polym. Degrad. Stab. 97, 1345–1354. https://doi.org/10.1016/j.polymdegradstab.2012.05.024.

Piñeros-Hernandez, D., Medina-Jaramillo, C., López-Córdoba, A., Goyanes, S., 2017. Edible cassava starch films carrying rosemary antioxidant extracts for potential use as active food packaging. Food Hydrocoll. 63, 488–495. https://doi.org/10.1016/j.foodhyd.2016.09.034.

Plastics Europe, 2024. The Circular Economy for Plastics: A European Analysis. Plastics Europe, Bruxelles.

Qin, J., Zeng, S., Wang, X., Lin, C., 2022. Generation of micro(nano)plastics and migration of plastic additives from Poly(vinyl chloride) in water under radiation-free ambient conditions. Chemosphere 299, 134399. https://doi.org/10.1016/j.chemosphere.2022.134399.

Rao, M.M., Botsa, S.M., Rao, T.P., Goddu, S.R., Vijayasanthi, C., 2024. A comprehensive review on agricultural waste production and onsite management with circular economy opportunities. Discov. Sustain. 5, 288. https://doi.org/10.1007/s43621-024-00492-z.

Remila, B., Zembouai, I., Zaidi, L., Yalaoui, K., Kaci, M., Kervoelen, A., Bruzaud, S., 2025. Performance Enhancement of Biocomposites Based on Poly (3-Hydroxybutyrate-Co-3-Hydroxyvalerate)/Polylactide Blend: Synergistic Effect of PHBV - *g* - MA Compatibilizer and Diss Fibers. J. Appl. Polym. Sci. 142, e57239. https://doi.org/10.1002/app.57239.

Saabome Samuel Muobom, Sangmyung University, Seoul, South Korea, 2020. Title: A Review on Plasticizers and Eco-Friendly Bioplasticizers: Biomass Sources and Market. IJERTV9IS050788 Int. J. Eng. Res. V9. https://doi.org/10.17577/IJERTV9IS050788.

Saffian, H.A., Yamaguchi, M., Ariffin, H., Abdan, K., Kassim, N.K., Lee, S.H., Lee, C.H., Shafi, A.R., Humairah Alias, A., 2021. Thermal, Physical and Mechanical Properties of Poly(Butylene Succinate)/Kenaf Core Fibers Composites Reinforced with Esterified Lignin. Polymers 13, 2359. https://doi.org/10.3390/polym13142359.

Salmah, H., Romisuhani, A., Akmal, H., 2013. Properties of low-density polyethylene/palm kernel shell composites: Effect of polyethylene co-acrylic acid. J. Thermoplast. Compos. Mater. 26, 3–15. https://doi.org/10.1177/0892705711417028.

Santandrea, D., Beghetto, V., 2025. 4-(4,6-Dimethoxy-1,3,5-triazin-2-yl)-4-methylmorpholinium chloride-assisted amide crosslinking of carboxymethyl cellulose for high-performing films. RSC Adv. 15, 34846–34860. https://doi.org/10.1039/D5RA05273D.

Santandrea, D., Sillard, C., Rey, C., Beghetto, V., Bras, J., 2026. Influence of aliphatic amine grafting on the barrier properties of TEMPO-CNF films, 10.1039.D6PY00462H Polym. Chem.. https://doi.org/10.1039/D6PY00462H.

Santhosh, N., Praveena, B.A., Gowda, A.C., Duhduh, A.A., Rajhi, A.A., Alamri, S., Berwal, P., Khan, M.A., Wodajo, A.W., 2024. Innovative eco-friendly bio-composites: A comprehensive review of the fabrication, characterization, and applications. Rev. Adv. Mater. Sci. 63, 20240057. https://doi.org/10.1515/rams-2024-0057.

Self, J.L., Zervoudakis, A.J., Peng, X., Lenart, W.R., Macosko, C.W., Ellison, C.J., 2022. Linear, Graft, and Beyond: Multiblock Copolymers as Next-Generation Compatibilizers. JACS Au 2, 310–321. https://doi.org/10.1021/jacsau.1c00500.

Shakoor Shar, A., Wang, N., Chen, T., Zhao, X., Weng, Y., 2023. Development of PLA/Lignin Bio-Composites Compatibilized by Ethylene Glycol Diglycidyl Ether and Poly (ethylene glycol) Diglycidyl Ether. Polymers 15, 4049. https://doi.org/10.3390/polym15204049.

Silva, L.M.R.D., Figueiredo, E.A.T.D., Ricardo, N.M.P.S., Vieira, I.G.P., Figueiredo, R.W. D., Brasil, I.M., Gomes, C.L., 2014. Quantification of bioactive compounds in pulps and by-products of tropical fruits from Brazil. Food Chem. 143, 398–404. https://doi.org/10.1016/j.foodchem.2013.08.001.

Silvia, Lisci, Stefania, Tronci, Massimiliano, Grosso, Henrik, Karring, Ron, Hajrizaj, Massimiliano, Errico, 2022. Brewer s Spent Grain: Its Value as Renewable Biomass and Its Possible Applications. Chem. Eng. Trans. 92, 259–264. https://doi.org/10.3303/CET2292044.

Sin, L.T., Bee, S.-T., Tee, T.-T., Kadhum, A.A.H., Ma, C., Rahmat, A.R., Veerasamy, P., 2013. Characterization of α-tocopherol as interacting agent in polyvinyl alcohol–starch blends. Carbohydr. Polym. 98, 1281–1287. https://doi.org/10.1016/j.carbpol.2013.07.069.

Singh, S., Tiwari, R.R., 2025. Micro/nanoplastics and human health: A review of the evidence, consequences, and toxicity assessment. Food Chem. Toxicol. 203, 115595. https://doi.org/10.1016/j.fct.2025.115595.

Soccio, M., Dominici, F., Quattrosoldi, S., Luzi, F., Munari, A., Torre, L., Lotti, N., Puglia, D., 2020. PBS-Based Green Copolymer as an Efficient Compatibilizer in Thermoplastic Inedible Wheat Flour/Poly(butylene succinate) Blends. Biomacromolecules 21, 3254–3269. https://doi.org/10.1021/acs.biomac.0c00701.

Song, X., Zhang, C., Yang, Y., Yang, F., Weng, Y., 2023. Cardanol derivatives as compatibilizers for strengthening and toughening polylactic acid/bamboo fiber biocomposites. Polym. Compos. 44, 5675–5688. https://doi.org/10.1002/pc.27518.

Souza, A., Arias, E., Arellano, V., Macarin, G., Vargha, S., Raggio, L.Ma, 2025. Revaluation of a beer industry by-product towards the development of a sustainable product: beer by-product pasta. Front. Food Sci. Technol. 5, 1491253. https://doi.org/10.3389/frfst.2025.1491253.

Spinelli, S., Conte, A., Lecce, L., Padalino, L., Del Nobile, M.A., 2016. Supercritical carbon dioxide extraction of brewer's spent grain. J. Supercrit. Fluids 107, 69–74. https://doi.org/10.1016/j.supflu.2015.08.017.

Surendren, A., Mohanty, A.K., Liu, Q., Misra, M., 2022. A review of biodegradable thermoplastic starches, their blends and composites: recent developments and opportunities for single-use plastic packaging alternatives. Green. Chem. 24, 8606–8636. https://doi.org/10.1039/D2GC02169B.

Turco, R., Mallardo, S., Zannini, D., Moeini, A., Serio, M.D., Tesser, R., Cerruti, P., Santagata, G., 2024. Dual role of epoxidized soybean oil (ESO) as plasticizer and chain extender for biodegradable polybutylene succinate (PBS) formulations. Giant 20, 100328. https://doi.org/10.1016/j.giant.2024.100328.

Visco, A., Scolaro, C., Facchin, M., Brahimi, S., Belhamdi, H., Gatto, V., Beghetto, V., 2022. Agri-Food Wastes for Bioplastics: European Prospective on Possible Applications in Their Second Life for a Circular Economy. Polymers 14, 2752. https://doi.org/10.3390/polym14132752.

Visco, A., Scolaro, C., Oliveri, F., Ruta, A.J., 2024. Mathematical Modelling of Tensile Mechanical Behavior of a Bio-Composite Based on Polybutylene-Succinate and Brewer Spent Grains. Polymers 16, 2966. https://doi.org/10.3390/polym16212966.

Visco, A., Bardella, N., Scolaro, C., Belhamdi, H., Brahimi, S., Gatto, V., Samiolo, R., Beghetto, V., 2025. Reuse of beer spent grain for the industrial production of biodegradable bio-composites. Ind. Crops Prod. 235, 121684. https://doi.org/10.1016/j.indcrop.2025.121684.

Visco, A., Scolaro, C., Brahimi, S., Conca, S., Beghetto, V., 2026. Effect of α-tocopherol on the processability, tensile properties, and structure of fully bio-based poly (butylene succinate)/Brewer's spent grain composites. Mater. Today Commun. 53, 115413. https://doi.org/10.1016/j.mtcomm.2026.115413.

Walker, T.R., Fequet, L., 2023. Current trends of unsustainable plastic production and micro(nano)plastic pollution. TrAC. Trends Anal. Chem. 160, 116984. https://doi.org/10.1016/j.trac.2023.116984.

Wang, X., Yang, D., Gan, L., Zhang, H., Shin, J., Lee, Y., Jang, Y., Lee, K., 2015. Effect of Positional Distribution of Linoleic Acid on Oxidative Stability of Triacylglycerol Molecules Determined by^{1} H NMR. J. Am. Oil Chem. Soc. 92, 157–165. https://doi.org/10.1007/s11746-015-2590-y.

Watson, P.F., Petrie, A., 2010. Method agreement analysis: a review of correct methodology. Theriogenology 73, 1167–1179. https://doi.org/10.1016/j.theriogenology.2010.01.003.

Winiarska, E., Jutel, M., Zemelka-Wiacek, M., 2024. The potential impact of nano- and microplastics on human health: understanding human health risks. Environ. Res. 251, 118535. https://doi.org/10.1016/j.envres.2024.118535.

Zheng, Y., Zheng, M., Ma, Z., Xin, B., Guo, R., Xu, X., 2015. Sugar Fatty Acid Esters. in: Polar Lipids. Elsevier, pp. 215–243. https://doi.org/10.1016/B978-1-63067-044-3.50012-1.